Remote Sensing of Environment 154 (2014) 378–386

Contents lists available at ScienceDirect

Remote Sensing of Environment

journal homepage: www.elsevier.com/locate/rse

An efficient, multi-layered crown delineation algorithm for mapping individual tree structure across multiple ecosystems

L.I. Duncanson [a,*], B.D. Cook [b], G.C. Hurtt [a], R.O. Dubayah [a]

[a] Department of Geographical Sciences, University of Maryland, 2181 Lefrak Hall, College Park, MD 20742, USA
[b] Goddard Space Flight Center, Greenbelt, MD, USA

ARTICLE INFO

Article history:
Received 1 April 2013
Received in revised form 1 July 2013
Accepted 24 July 2013
Available online 6 April 2014

Keywords:
LiDAR
Forest
Individual tree structure
Crown delineation
Carbon

ABSTRACT

Deriving individual tree information from discrete return, small footprint LiDAR data may improve forest aboveground biomass estimates, and provide tree-level information that is important in many ecological studies. Several crown delineation algorithms have been developed to extract individual tree information from LiDAR point clouds or rasterized canopy height models (CHM), but many of these algorithms have difficulty discriminating between overlapping crowns, and also may fail to detect understory trees. Our approach uses a watershed-based delineation of a CHM, which is subsequently refined using the LiDAR point cloud. Individual tree detection was validated with stem mapped field data from the Smithsonian Environmental Research Center (SERC), Maryland, and on a plot and stand level through comparisons of stem density and basal area to delineated metrics at both SERC and a study area in the Sierra Nevada, California. For individual tree detection, the algorithm correctly identified 70% of dominant trees, 58% of codominant trees, 35% of intermediate trees and 21% of suppressed trees at SERC. The algorithm had difficulty distinguishing between crowns of small, dense understory trees of approximately the same height. Delineated crown volume alone explained 53% and 84% of the variability in basal area at the SERC and Sierra Nevada sites, respectively. The algorithm produced crown area distributions comparable to diameter at breast height (DBH) size class distributions observed in the field in both study sites. The algorithm detected understory crowns better in the conifer-dominated Sierra Nevada site than in the closed-canopy deciduous site in Maryland. The ability for the algorithm to reproduce both accurate tree size distributions and individual crown geometries in two dissimilar and complex forests suggests great promise for applicability to a wide range of forest systems.

1. Introduction

LiDAR has become the dominant technology for mapping 3D forest structure (Wulder et al., 2012; Zolkos, Goetz, & Dubayah, 2013). Discrete return and waveform LiDAR have been widely applied for forest height, crown volume and biomass estimation. While medium or large footprint (20–70 m) LiDAR data are useful for characterizing the vertical distribution of canopies at the resolution of the footprint, small footprint (10s of cm) LiDAR provides both vertical and horizontal information at the scale of individual trees (Wulder et al., 2012). Estimates of forest biomass have largely ignored the highly detailed spatial information from discrete return LiDAR and focused on metrics such as canopy height and cumulative vertical distributions at plot level, as in Chen, Gong, Baldocchi and Tian (2007); Popescu, Wynne and Nelson (2003); and Popescu (2007). Providing more spatially detailed information such as the number, location, spacing, and size distribution of individual trees may improve biomass estimation at varying spatial resolutions, and should provide a more ecologically meaningful structural description of a forest.

Various methods for extracting individual tree information from high resolution LiDAR datasets have been developed. These techniques generally fall into three categories: local maxima detection and expansion (Kaartinen et al., 2012; Leckie et al., 2003; Maltamo, Mustonen, Hyyppa, Pitkanen, & Yu, 2004; Persson, Holmgren, & Soderman, 2002; Popescu & Wynne, 2004; Vastaranta et al., 2011; Wulder, Niemann, & Goodenough, 2000), watershed-based delineation (Breidenbach, Næsset, Lien, Gobakken, & Solberg, 2010; Chen, Baldocchi, Gong, & Kelly, 2006; Koch, Heyder, & Weinacker, 2003; Kwak, Lee, Lee, Biging, & Gong, 2007), and point-cloud clustering (Ferraz et al., 2012; Rahman & Gorte, 2009). Local maxima algorithms typically involve the selection of a search radius and detection of local maxima from a CHM. Popescu and Wynne (2004) used both circular and square windows with site-specific window sizes to increase local accuracy of maxima detection. Leckie et al. (2003) applied a valley-following approach to isolate crowns based on CHM topography that yielded both tree

* Corresponding author. Tel.: +1 301 256 4302.
E-mail address: lduncans@umd.edu (L.I. Duncanson).

http://dx.doi.org/10.1016/j.rse.2013.07.044
0034-4257/

locations and crown geometries with 80% accuracy. However, the trees in this study were well spaced and easily visible in the CHM. Vastaranta et al. (2011) used a minimum curvature approach with local maxima detection for a boreal forest and although they did not present an individual tree accuracy, they used delineated crowns to predict basal area ($R^2 = 0.48$) and volume ($R^2 = 0.71$). Maltamo et al. (2004) also worked in a boreal forest with a local maxima detection algorithm and reported that while as much as 80% of dominant crowns were correctly detected, the total accuracy was 40% due to issues identifying understory crowns. Although local maxima techniques are computationally the fastest and simplest algorithms, these algorithms often fail to detect understory and overlapping trees in structurally complex forests, and have difficulty detecting crown edges, typically oversimplifying crown geometry (Kaartinen et al., 2012).

Watershed-based delineations offer an improvement for crown geometries, and function on inverted CHMs by segmenting neighboring crowns along lines of local minima (Chen et al., 2006). Watershed approaches can be combined with local maxima detection to limit the number of local maxima within a segment to one. Koch et al. (2003) used a modified watershed approach, allowing for merging and refinement of delineations with *a priori* knowledge of forest structure. They found that for conifer trees, approximately 87% of trees were correctly identified using this technique but for deciduous species only 50% were correctly delineated, with errors arising from understory and overlapping crowns. Breidenbach et al. (2010) also found that their watershed approach could not detect understory or overlapping crowns when local maxima were undetected.

Point cloud based techniques are the newest and most computationally demanding of the three delineation approaches. Point cloud-based techniques use the full information content from discrete return LiDAR datasets and therefore offer great promise for future advancement in this field. However, current point cloud-based techniques have focused on small areas within a single study site and may not be applicable across a range of forest types. Rahman and Gorte (2009) use the density of LiDAR returns for crown detection, while Ferraz et al. (2012) use an iterative clustering approach based on a mean shift algorithm to detect trees in 3D space. Ferraz et al. (2012) reported that although 99% of overstory trees were detected by their algorithm, only 12.8% of suppressed trees were detected, suggesting that even detailed site-specific point cloud methods have difficulty detecting understory trees.

Most algorithms for crown delineation have remained focused on conifer dominated, boreal forests, with plot level validation. Kaartinen et al. (2012) conducted an analysis of several delineation algorithms in boreal systems and reported accuracies that range from 40 to 95% for open conifer trees, 5–45% for trees neighboring a larger tree, and less than 20% for intermediate or suppressed canopies. Boreal forests are less structurally complex than temperate or tropical broadleaf forests, and therefore algorithms developed in boreal areas may be less effective in more complex forests. Current crown delineation algorithms inadequately identify understory and overlapping trees, and have rarely been tested across different biomes. There is consequently a need for an understory-sensitive algorithm that can be efficiently applied to LiDAR datasets with a range of point densities in a variety of ecosystems. The goal of this paper is to present the development and testing of a novel crown delineation algorithm that offers both applicability over varying forest types and improvement for understory and overlapping tree detection.

2. Methods

2.1. Study areas

Our delineation algorithm is tested in the eastern and western USA. The first study site is a broadleaf dominated experimental forest in Maryland managed by the Smithsonian Environmental Research Center (SERC). SERC is located near Edgewater, Maryland, adjacent to a subestuary of the Chesapeake Bay. The area is generally comprised of two forest types: mature secondary upland forest and floodplain forests. Dominant species in the upland forest include tulip poplar, several species of oak, beech, and several species of hickory, with mid canopy red maple and sour gum and understory American hornbeam, spicebush and paw-paw. Dominant species in the flood plain area are ash, sycamore, and American elm. Both the upland and the floodplain forests have been relatively undisturbed for approximately 120 years.

The second study site is the Teakettle Experimental Forest in the western Sierra Nevada mountain range, California. Dominant species include California black oak, white fir, ponderosa pine and red fir (Hunsaker, Boroski, & Steger, 2002). The elevation ranges from approximately 1000 m to 2500 m, with aboveground biomass values averaging ~200 Mg/ha with individual trees up to 20.0 Mg. The forest is mature, featuring clusters of trees in flatter areas of the land with thicker soils, and rocky outcrops in steeper areas (Swatantran, Dubayah, Roberts, Hofton, & Blair, 2011).

2.2. Field data

In the SERC study area, field data were taken from the SIGEO field acquisition, in which a 16.0 ha plot was laid out and every tree greater than 1 cm DBH was sampled and stem mapped between 2008 and 2011 (http://www.sigeo.si.edu/). Tree location, species, DBH, crown class (dominant, codominant, intermediate or suppressed) and crown condition were recorded. Dead and damaged trees were eliminated from the dataset prior to comparison with delineation results due to a lack of description of the type of damage. For validation, the 16 ha stem map was subset into 16, 90 meter square subplots. The stem map at SERC is based on georegistered based on a series of monumented posts that were located every 200 m on a true N–S geographic grid. The location of these posts had an accuracy of less than 1–2 m. Additional posts were located at 10 by 10 meter spacing within the SIGEO area, and trees were stem mapped using measuring tapes. The additional posts were laid out using a combination of laser rangefinders and compasses, as well as a total station (Parker, G., Pers. Comm.).

In the Teakettle forest area, 90 m square sample plots were collected in the summer of 2008 ($n = 12$). The DBH, species and condition of all trees were recorded. Dead trees were removed from the analysis. Within each central sub-plot the location and height of trees were also recorded. However, given issues with georegistering tree locations to LiDAR data, stem mapped data were not used to pursue an individual-based tree validation for the Sierra Nevada site.

2.3. LiDAR data

LiDAR data for SERC were collected with NASA Goddard's LiDAR, Hyperspectral and Thermal Imager (Cook et al., 2013) instrument. G-LiHT uses a 300 kHz multi-stop scanning LiDAR with a 60° field of view and 10 cm diameter footprint, and the site was flown with 50% overlap in north–south and east–west directions to achieve a mean return density of up to 50 laser pulses/m^2. Leaf-off and leaf-on data were acquired during March, 2012 and June, 2012, respectively.

LiDAR data for the Sierra Nevada site were flown in the summer of 2008 with the University of Florida's OPTECH GEMINI ALSM unit, operating at 100–125 kHz with a maximum 25° scanning angle. Data were flown ~600–750 m above ground, with 50%–75% swath overlap yielding an average return density of approximately 18 pts/m^2.

2.4. Algorithm development

Fig. 1 shows the processing framework applied by our algorithm. The only inputs to the algorithm are raw LiDAR point cloud files. These LiDAR point clouds are preprocessed adding a 20 m buffer to LiDAR tiles to ensure that tile edges do not affect the outputs. The

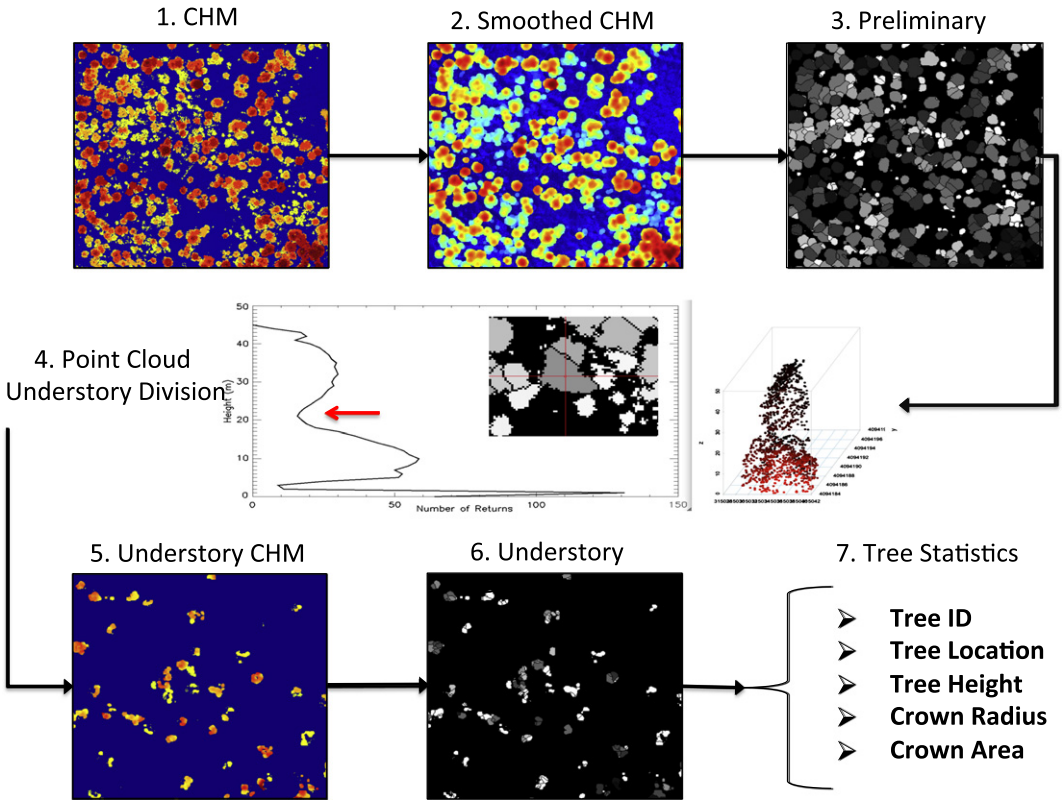

Fig. 1. Processing flow of algorithm. First a CHM is generated. Second, the CHM is smoothed and internal crown gaps are filled. Third, a preliminary watershed delineation is applied. Fourth, the raw LiDAR returns from each segmented area are extracted and binned vertically, a trough finding algorithm is applied, and returns are classified as either overstory or understory. Fifth, overstory and understory CHMs are generated. Sixth, the overstory and understory CHMs are segmented. Steps 4–6 are applied iteratively. Finally, tree statistics are generated.

algorithm generates a series of rasters with a 0.5 m pixel size. The first raster, a Digital Terrain Model (DTM), is generated using all returns with a moving window and local minima detection and smoothing. The second raster, a canopy height model (CHM), is generated by finding the maximum Z value (from all returns) in each pixel and subtracting the corresponding DTM value (Fig. 1.1). This raw CHM is then smoothed using a customized moving window average filter (Fig. 1.2). The window size can be varied, but a 5 by 5 window was used here.

The customized smoothing algorithm is described as follows. First, pixels are classified as canopy or ground pixels using 2 m as a separation between canopy and potential ground hits. Ground pixels are not included in averaging to avoid underestimating tree heights. For each 'ground' pixel, the algorithm searches neighboring pixels to determine whether the pixel is within a crown or outside of a crown. If four or more neighboring pixels are canopy pixels, the central pixel will be classified as a within crown low return. These pixels are assigned the average value of their neighboring crown pixels to reduce over segmentation of crowns due to either high return density LiDAR or sparse canopies. It should be noted that the 2 m height filter means that this algorithm does not detect understory vegetation at less than 2 m of height.

After smoothing, a preliminary delineation is conducted using an inverted CHM and a watershed function (Fig. 1.3). Every pixel in the image is assigned the ID number of the associated watershed. Pixels with an elevation less than 2 m are assigned as ground pixels, and set to a value of zero.

The preliminary watershed segments may represent a single tree or a cluster of trees. To separate returns from understory trees, the raw point cloud data are extracted for the area overlapping each preliminary segment (Fig. 1.4). These raw points are binned with a vertical resolution of 10 cm, generating a LiDAR height histogram for each preliminary segment. A trough finding algorithm smoothes the height histogram and detects troughs by determining when there is a continuous decrease and subsequent continuous increase in bin magnitude for a moving window of 9 bins (Fig. 2). When multiple troughs are detected the highest trough is selected as the point of return separation. It is assumed that there will be no significant troughs found in height histograms returned from a single tree, and that there will be a trough found before the peak return from lower trees in the case of tree clusters. Fig. 2 shows four examples of this point cloud refinement.

The LiDAR returns below each detected trough are separated from the higher LiDAR returns. Each set of returns is then used to generate two new CHMs for the entire area, one of higher canopies, and one of lower canopies (Fig. 1.5). These secondary canopy height models are then segmented with another watershed delineation, resulting in the separation of tree clusters and the delineation two layers of tree crowns (Fig. 1.6). If there are only two layers in a system, an overstory and an understory set of tree crowns will be detected. In the case of multilayered forests, the process of generating height histograms, separating vertical returns, and generating understory canopy height models, is iterated until no further understory trees are detected. Therefore this algorithm is capable of detecting infinite layers of tree crowns, however in both of the systems in this study, three layers were detected. Therefore we will refer to the first layer as an 'overstory' layer, the second as a 'midstory' layer, and the third as an 'understory' layer.

The location, height, area, and radius of trees are generated from the algorithm (Fig. 1.7). Crown area is calculated as the number of pixels in the crown multiplied by the area per pixel (0.25 m^2). Crown radius was computed as the mean crown radius along the north–south and east–west directions. Tree heights were extracted from the unsmoothed CHM corresponding to the canopy layer. For example, if the algorithm is run for three layers, tree segments from the highest layer are assigned heights from the overstory CHM, tree segments from the middle layer

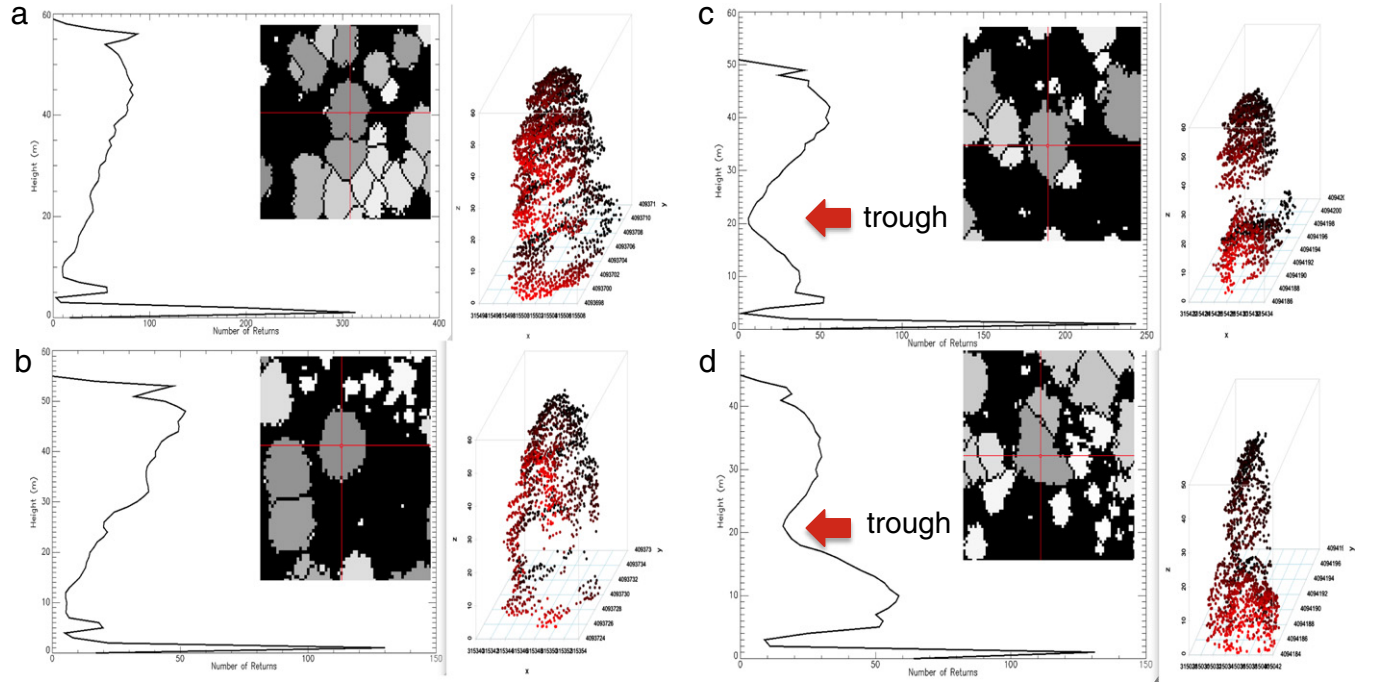

Fig. 2. Four examples of point cloud extraction and binning showing the preliminary segment location under the red crosshairs, the extracted LiDAR returns with red indicating distance in Y, and the corresponding vertically binned pseudo waveforms. a) and b) were determined to be individual trees while c) and d) were flagged as multiple trees. The returns below the indicated troughs were separated for generation of an understory CHM.

are assigned heights from the mid layer CHM, and tree segments from the lowest layer are assigned heights from the lowest, or understory, CHM.

Fig. 3 illustrates the potential power of multilayered crown delineation. A few tall trees in the original CHM resulted in preliminary segments representing clusters of trees rather than individuals. Separating the tall trees for processing as overstory crowns allowed for shorter crowns to be correctly detected and delineated.

Although this algorithm is computationally demanding, it has been optimized for use in parallel computing systems resulting in computational efficiency. 32 cores (CPUs), each with 2GB RAM processed the SERC dataset in 1.5 h and the Sierra Nevada dataset in 30 min. The algorithm is written in IDL and GDL, and could be run in serial however it would take at least 32 times longer to run (~32 h) for these relatively small areas. This algorithm was run on NASA's Pleiades supercomputing system through affiliations with the NASA Earth Exchange (https://c3.nasa.gov/nex/).

2.5. Algorithm validation

The purpose of the validation was both to determine the overall accuracy of the model, and to determine whether certain tree size classes are being captured more accurately than others. This was performed both on an individual tree level, at SERC, and at a plot and stand level at both SERC and in the Sierra Nevada site.

Individual tree validation was performed through matching delineated crowns to stem mapped trees at SERC. For each tree greater than 5 cm DBH in the SERC field dataset, a variable search radius was applied based on crown class. This is because there will be a tighter link between stem and crown centroid for smaller trees than for larger trees. Search radii were 8.0 m, 6.0 m, 4.0 m and 2.0 m, for dominant, codominant, intermediate and understory crowns, respectively. The LiDAR data was searched for each field observed tree to determine if there was a detected tree of the given size class in the given search radius. The size of a detected tree was deemed correct if the crown area in m^2 was within +/− 50% of the DBH in cm (Fig. 8). The 50% margin allows for stem to crown allometric variability. If more than one tree in the correct size was found, the closer tree was considered a match and removed from the LiDAR dataset to prevent matching with other trees from the field dataset. If no tree of the correct size class was found within the search radius, it was marked as an error of omission. Once the LiDAR dataset had been parsed of matched trees, the remaining trees were marked as errors of commission. This analysis was repeated for both the leaf-on and leaf-off SERC LiDAR datasets to address the algorithm's sensitivity to the season of data collection.

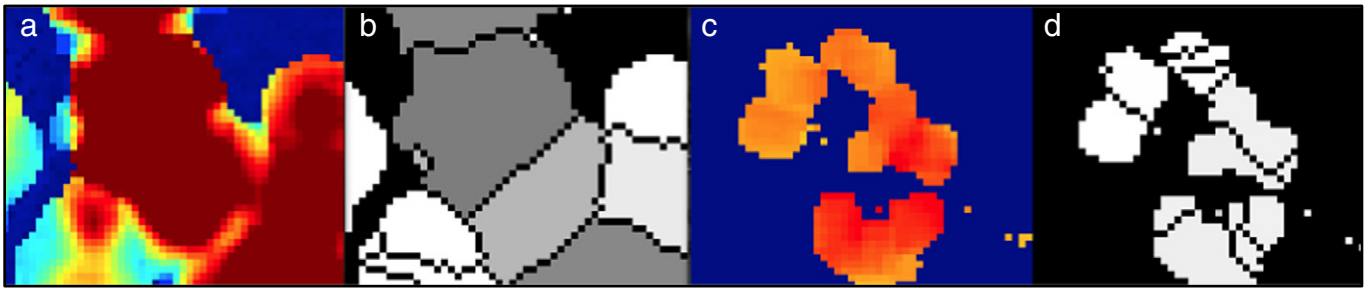

Fig. 3. a) Smoothed CHM, b) preliminary segmentation, c) understory CHM and d) understory segmentation. The shorter trees seen in the c) and d) were not apparent in the original CHM because of taller overstory trees.

Table 1
Individual tree level reported accuracies at the SERC study site. The % correct is the number of corrected identified stems divided by the total number of stems from the field dataset. The % Estimated is the number of total identified stems (correct and errors of commission) divided by the total number of stems in the field.

		March	June
% correct	Dominant	56%	70%
	Codominant	52%	58%
	Intermediate	32%	35%
	Suppressed	29%	21%
% estimated	Dominant	56%	70%
	Codominant	98%	103%
	Intermediate	199%	201%
	Suppressed	58%	50%

Plot level validation was conducted by comparing the number of stems and basal area from field datasets to the number of stems, cumulative crown area, and cumulative crown volume derived from the crown delineation. Delineated crowns were extracted for each of the plot areas. Cumulative area was calculated as the sum of crown areas in each field plot. Cumulative volume was calculated as the sum of crown area multiplied by tree maximum height. Relationships between field observed crown radius and DBH were applied to DBH field datasets in order to determine stand level differences between field observations and delineated metrics. A crown diameter model was developed using limited crown geometry data at Teakettle. At SERC, a model between crown radius and DBH was developed by Parker, G. (Pers. Comm.). These models were applied to field observed DBH to produce estimates of crown radius and area for both field datasets.

Stand level validation was then conducted by analyzing the histograms of delineated crown areas to histograms of field observed DBHs and generating quantile–quantile plots of field estimated crown area against delineated area. For this comparison, delineated data were stripped to the area of field data collection. At SERC, data were stripped to the square 16 ha stem mapped area.

3. Results

3.1. Individual tree level validation

At SERC, the number of trees correctly detected in each crown class in June, as a percentage of number of stems in the field dataset, is 70% dominant trees, 58% codominant trees, 35% intermediate trees and 21% of suppressed trees (Table 1, Fig. 4).

To test the algorithm's sensitivity to leaf-off versus leaf-on LiDAR data collection, two data collection periods were compared. Fig. 5 shows the accuracy of individual tree detection in SERC during the

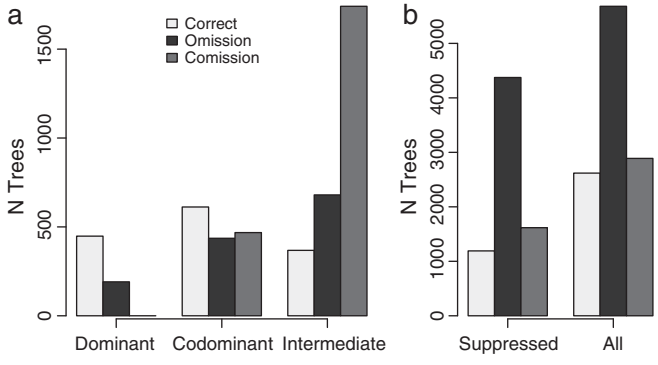

Fig. 4. The individual tree-based accuracy assessment at SERC during the leaf-on period showing the number of trees correctly classified as well as errors of omission and commission. a) Comparisons for dominant, co-dominant and intermediate classes and b) suppressed and total errors.

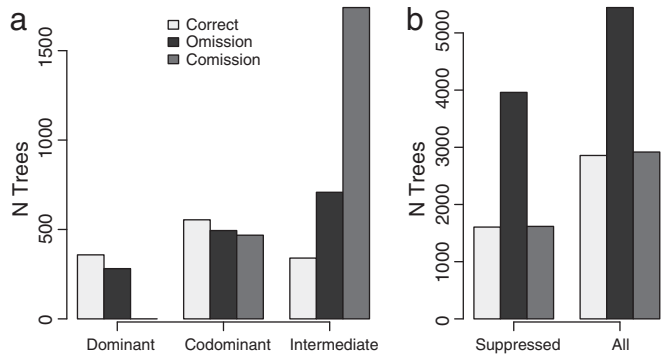

Fig. 5. Individual tree-based accuracy assessment during leaf-off period at SERC. a) Shows comparisons for dominant, co-dominant and intermediate classes and b) shows suppressed and total errors.

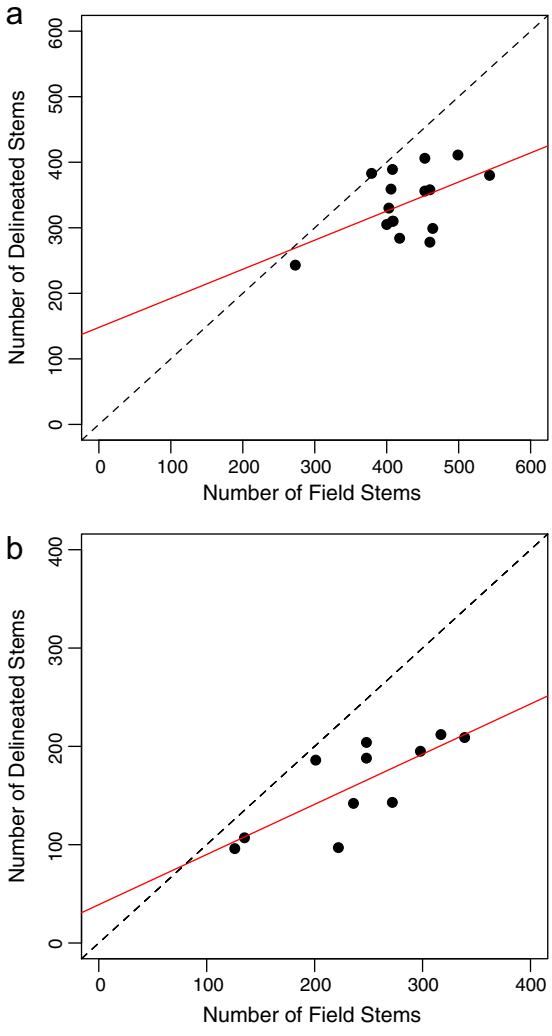

Fig. 6. Number of stems in the field compared to number of stems estimated by the algorithm at the 90 meter plot level in a) the SERC site and b) the Sierra Nevada site. The dotted line shows the 1:1 line, illustrating an underestimation of stem density at both sites. This is attributed to the algorithm failing to detect some small stems.

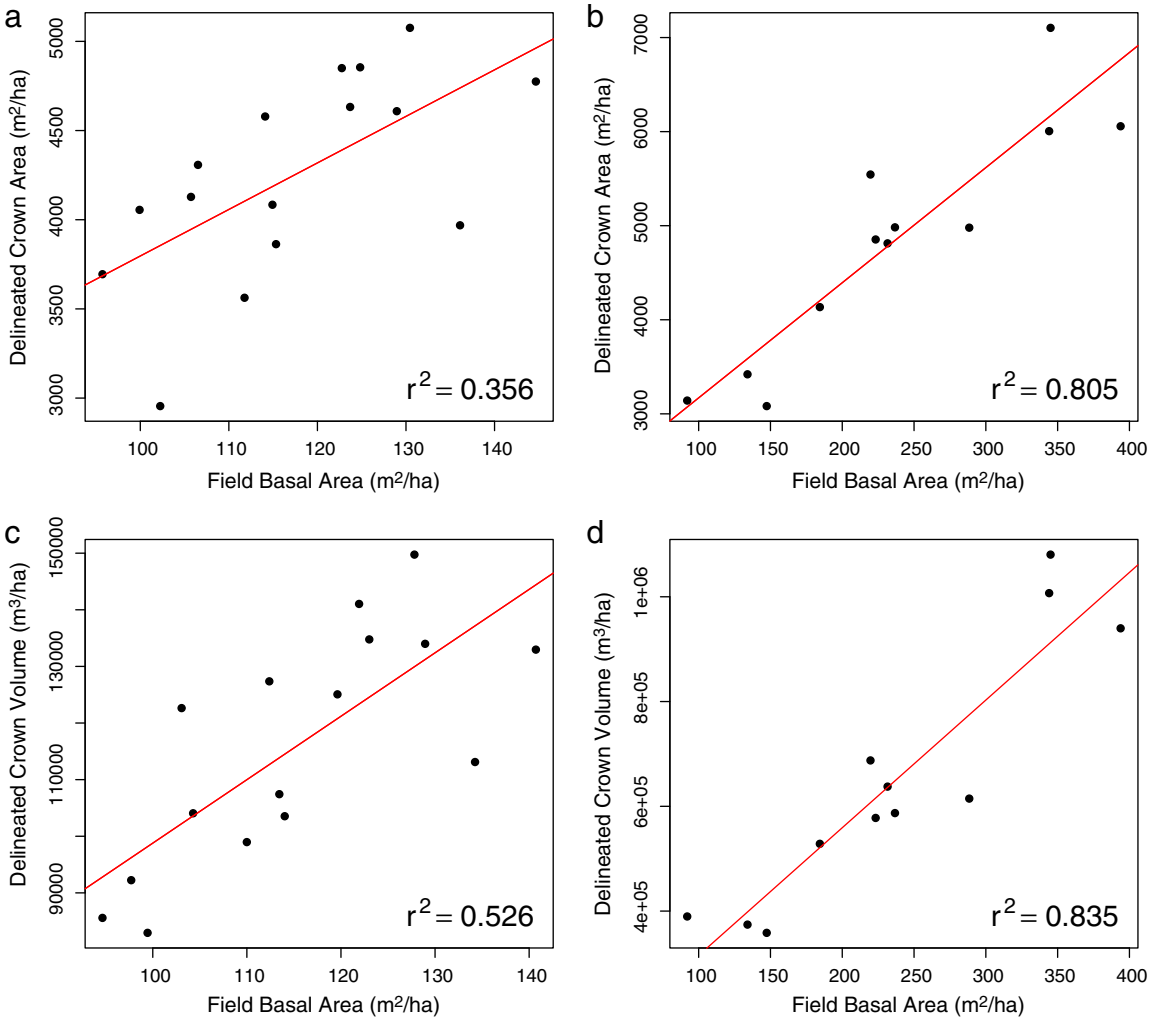

Fig. 7. Field estimates of basal area compared to cumulative crown area at a) SERC site, b) Teakettle and cumulative crown volume (area * height) at c) SERC and d) Teakettle.

leaf-off period. Overall, the algorithm performs similarly in both leaf-on and leaf-off conditions (Table 1). However, 14% fewer dominant trees are correctly detected during leaf off, while 8% more suppressed trees are correctly identified.

3.2. Plot level validation

The utility of the algorithm for plot-level ecological properties such as stand density and basal area is demonstrated in Figs. 6 and 7. Stem

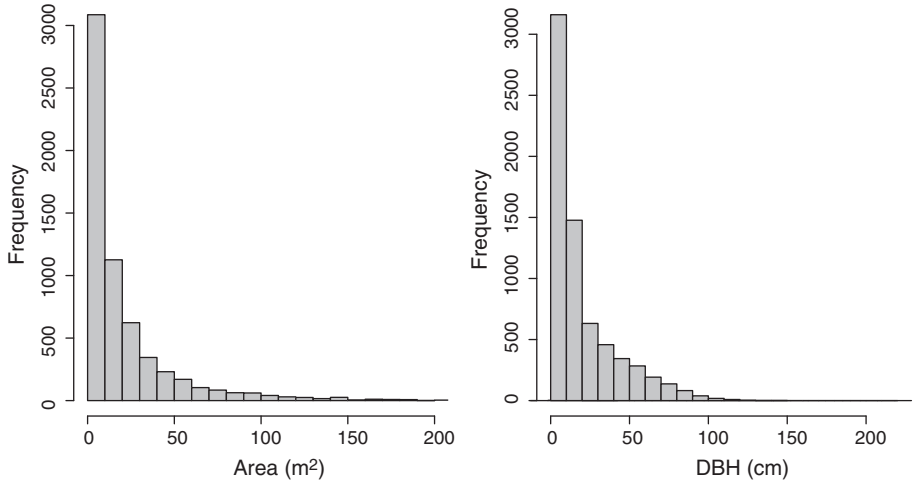

Fig. 8. Histograms of delineated crown area (left) and DBH (right) for SERC site showing that the shape of the histograms matches closely although there is an underestimation in the smallest trees by the algorithm.

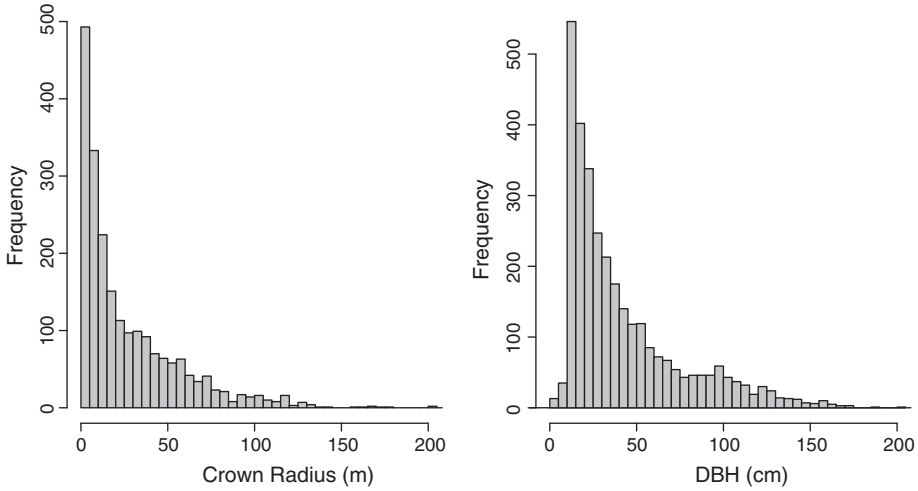

Fig. 9. The histograms of delineated crown area (left) and DBH (right) for the Sierra Nevada site, showing that the shape matches well and DBH in cm is approximately comparable to area in m^2.

density was underestimated at both the SERC and Sierra Nevada sites. On average stem density is underestimated by 20% at the SERC site (Fig. 6a) and 32% at the Sierra Nevada site (Fig. 6b), the majority of this estimation being from undetected small trees.

There is a stronger relationship between plot level cumulative delineation metrics and basal area at Teakettle than at SERC (Fig. 7). R^2 values between basal area and crown area were 0.36 and 0.81 at SERC and Teakettle, respectively. R^2 values were higher for crown volume: 0.53 and 0.84, at SERC and Teakettle, respectively.

3.3. Stand level validation

The shape of the tree size distributions is well captured at both study sites, as seen in the histograms of crown area and DBH (Figs. 8, 9). To make a more direct comparison between field and delineated datasets, two species independent DBH-crown diameter models were applied. The relationship between DBH and crown diameter at SERC was diameter $= (0.39 * \text{DBH}) * (1 - \exp(-\text{DBH} * 0.44))$. The relationship developed between crown diameter and DBH at Teakettle was diameter $= 2.5 + 1.8 * \text{DBH}^{0.65}$ ($R^2 = 0.72$, RMSE $= 0.69$, n $= 281$). Each model was applied to the respective field dataset to produce field estimates of crown radius and area. Fig. 10 shows quantile–quantile plots of delineated crown areas against field-estimated areas at a) SERC and b) Teakettle.

At SERC our algorithm tends to underestimate crown area while at Teakettle there is a slight overestimation. However it is noteworthy that the near linear relationships shown in Fig. 10 indicate that stand level distributions were well captured at both sites. Only at very large (~150–200 m^2) crown sizes do the relationships between field and delineated distributions begin to falter. These results indicate that tree size distributions over large areas can be accurately estimated with our algorithm.

4. Discussion

4.1. Individual tree validation

The individual tree accuracies (Figs. 4, 5) compare favorably with other crown delineation results in deciduous systems that report ~50% accuracy for deciduous crowns (Koch et al., 2003). Intermediate and understory results are comparable to results from conifer-dominated systems that report less than 20% accuracy (Kaartinen et al., 2012). The algorithm therefore performs best for dominant and codominant trees, while intermediate trees are over predicted (commission) and understory trees are often undetected (omission).

Errors of commission are likely caused by the complex canopy structures found at SERC. In a closed deciduous forest, such as SERC, a single tree may be delineated into multiple crowns due to isolated branching units being falsely identified. This will be less common in conifer-dominated forests with conical crowns for which trees typically yield only one local maxima. Conversely, errors of omission at SERC are likely caused either by overlapping crowns of neighboring trees, or small understory trees from which few or no LiDAR hits are returned. In the first case, this algorithm may identify a cluster of trees as a preliminary segment (Fig. 3b) and the point cloud refinement may fail to subsequently separate these crowns. The utility of the point cloud refinement is strongly dependent on individual crowns yielding separate signals in vertical profile. Neighboring trees of a similar height with overlapping crowns will be merged by our algorithm because they will neither be separated by watershed segmentation (due to overlapping crowns) nor point cloud refinement (due to similar heights). This is one explanation for the overestimation of intermediate crowns: multiple neighboring suppressed trees in dense understory may be detected as an intermediate-sized crown rather than several smaller crowns. In the second case, the detection of small trees under dense canopies is limited for all airborne-based LiDAR delineations, without further improvements in technology and algorithms.

Understory tree detection is slightly improved when using leaf-off LiDAR data, but at the cost of decreasing the delineation accuracy of large crowns. This improvement is likely caused by the greater penetration of LiDAR hits both to the understory and the ground in leaf-off conditions. However, the increased penetration also causes more gaps within larger crowns, yielding more errors involving the detection of multiple crowns for a single large tree. Essentially, branching units are more likely to be detected as individual crowns when leaves are not present to fill in gaps between branches. This tradeoff should be considered when designing data collection campaigns focused on individual tree level information.

Despite difficulties detecting small crowns, 21% of all suppressed trees greater than 5 cm DBH are correctly identified at SERC. Given that SERC represents a challenging, closed-canopy forest our results suggest that this algorithm has utility across varies forest systems. If stem mapped data were available at Teakettle, accuracies at the individual level would likely be much higher, as suggested by numerous studies in conifer forests.

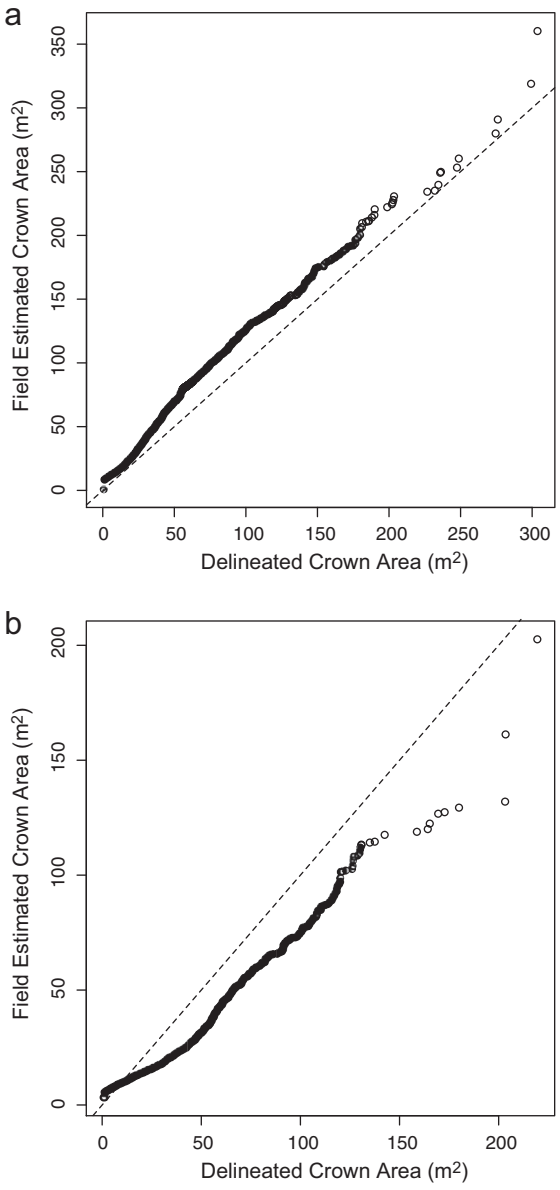

Fig. 10. Quantile–quantile plots of delineated crown areas against field estimated crown areas at a) SERC and b) Teakettle. The linear patterns observed in these figures suggest that the algorithm produces crown area distributions with the same shape as field derived distributions, with a slight underestimate in crown are at SERC and overestimate in crown area at Teakettle.

4.2. Plot level validation

Basal area is a structural attribute that has been widely studied due to both its commercial importance in forestry and high correlation to aboveground biomass for carbon mapping initiatives. The cross sectional area of a tree trunk should scale linearly with crown area, while basal area should scale with crown volume in the form of a power law with an exponent of 3/4 (Enquist, 2002). Therefore comparing crown areas and volumes to basal area is not only a reasonable approach for plot-level algorithm validation, but also allows for an assessment of how useful crown delineation might be for forestry and carbon mapping applications.

The relationship between basal area and crown area will depend largely on light environment. In an open system, tree crowns are not spatially limited and basal area increases will be reflected by corresponding increases in crown area and volume. In a closed-canopy environment, however, crown growth is often limited to light availability, and increases in biomass may be allocated disproportionally to stem vertical growth. Additionally, plot level cumulative canopy area will likely remain constant as basal area continues to increase, because crowns are limited in terms of lateral growth by their neighbors. Therefore discrepancies between plot level basal and crown area at SERC (Fig. 7a) are not solely explained by algorithm error. The stronger relationship at Teakettle can be explained either by higher algorithm accuracy in an open conifer site, or by a tighter link between crown and basal area in an open light environment.

Crown volume accounts for both increases in tree height and crown area as trees accumulate biomass. We therefore also compared crown volume to basal area with improved results (Fig. 7c, d). There is a stronger relationship at both sites between basal area and crown volume than with crown area. Again, the Sierra Nevada site shows a stronger relationship with crown volume than the SERC site, indicating that this algorithm performs better in the open conifer site. However, 53% of the basal area can be explained solely with delineated crown volume at the SERC site, suggesting that this approach may be useful for forestry and carbon applications even in closed canopy deciduous forests that present some of the most problematic conditions for crown delineation. In contrast, Lefsky, Harding, Cohen, Parker, and Shugart (1999) explained 69% of variability in basal area in a lower biomass area of SERC using stepwise regression of LiDAR-derived height and density metrics while we explain 53% with a single metric. This result, along with the strong relationship shown in Fig. 7d, suggests that this approach may be useful for biomass estimation and should be further explored for detailed carbon mapping initiatives.

4.3. Stand level validation

The algorithm reproduced the shape of the distribution of crown sizes observed in the field datasets at both sites. However, there was an apparent underestimation in crown area at SERC and overestimation at Teakettle. This was caused either by algorithm error, or error in the DBH-crown area equations developed from limited field data acquisitions at both sites. At Teakettle, for example, the DBH–crown area relationship was derived using 281 individual crowns, which did not capture the entire distribution of crown sizes across the stand. Additionally, the relationship was tighter for smaller crowns with great variability at larger stem sizes. Therefore the apparent overestimation in crown area from the algorithm may have been caused by an underestimation from the field dataset.

However, it is logical that there would be an underestimation in crown area at SERC. Closed canopy crowns often extend into neighboring crowns, potentially causing truncations in crown segmentation. This issue would not occur in open conditions such as found at Teakettle, explaining the discrepancy between the two systems.

Regardless of slight over or underestimations of crown areas, the linear relationships observed in the quantile–quantile plots demonstrate that stand level tree size distributions can be accurately produced from our crown delineation algorithm for both ecosystems.

This algorithm was developed with collaboration with NASA Ames and the NASA Earth Exchange (NEX). NEX is a program that allows scientists to take advantage of the large datasets and computing facilities available at NASA through remotely accessing their system. Although the goal of this paper was on algorithm development and validation rather than operationalization, large datasets could be processed using this algorithm, providing data to ecologists or forest managers interested in expanding the spatial scope of field data collections, adding crown-specific information that can be difficult to assess from the ground, or allowing consistent analysis of forest change through repeat pass LiDAR.

5. Conclusions

Airborne LiDAR remote sensing systems are increasingly being used to map large forested areas at high point density. The point clouds from these data result from the interaction of laser energy with trees, that are well-defined, discrete objects. It is therefore not surprising that so much effort has gone into the inverse problem of organizing these clouds back into trees. For a variety of applications, from habitat structure, to fire modeling, to biomass estimation, there are sound ecological reasons for doing so. However, the problem is a difficult one, and finding an algorithm with general efficacy across ecosystem structures has been challenging. The algorithm presented here is one further step in this direction.

Closed canopy broadleaf forests, such as SERC, and needle-leaf conifer forests, such as Teakettle, span a wide range of species functional types that result in markedly different spatial and vertical canopy structures, and as a result provided a reasonable test of accuracy and applicability. Considering that there was no change in parameterization between the two sites, our algorithm shows promise for wide applicability, with the potential to accurately extract crown information across systems. As computing capabilities and data storage facilities continue to improve, and high-resolution LiDAR datasets are increasingly available, trade-offs between spatial detail and area of coverage may no longer be necessary. Our algorithm, in tandem with high end computing, could be used to extract individual tree information at regional or even national levels given data availability. This algorithm therefore represents a shift toward detailed mapping over large areas, with the potential to provide unprecedented volumes of highly detailed structural information of great value for forest management, carbon and habitat mapping.

Acknowledgments

The authors gratefully acknowledge the NASA Earth and Space Science Fellowship program (grant number 016324-001), and the Natural Sciences and Engineering Research Council of Canada (NSERC), Postgraduate Graduate Scholarship D3, for funding this work. Thank you to the Smithsonian Environmental Research Center and SIGEO program for provision of field data. Specific thanks go to Dr. Geoffrey Parker for data provision and helpful comments on this manuscript. The algorithm was run on the Pleiades supercomputer at NASA Ames through the NASA Earth Exchange (NEX) program. NEX represents a new platform for the Earth science community that provides a mechanism for scientific collaboration and knowledge sharing. NEX combines state-of-the-art supercomputing, Earth system modeling, workflow management, NASA remote sensing data feeds, and a knowledge sharing platform to deliver a complete work environment in which users can explore and analyze large datasets, run modeling codes, collaborate on new or existing projects, and quickly share results among the Earth Science communities. Additional thanks go to Dr. Matthew Brolly, Dr. Naiara Pinto, Dr. Anu Swatatran, Dr. James Kellner, Dr. Jackie Rosette, Justin Fisk, Katelyn Dolan, Benjamin Stewart, the members of the Global Ecology Lab and all those who collected the field data.

References

Breidenbach, J., Næsset, E., Lien, V., Gobakken, T., & Solberg, S. (2010). Prediction of species specific forest inventory attributes using a nonparametric semi-individual tree crown approach based on fused airborne laser scanning and multispectral data. *Remote Sensing of Environment, 114*(4), 911–924.

Chen, Q., Baldocchi, D., Gong, P., & Kelly, M. (2006). Isolating individual trees in a savanna woodland using small footprint LiDAR data. *Photogrammetric Engineering and Remote Sensing, 72*(8), 923–932.

Chen, Q., Gong, P., Baldocchi, D., & Tian, Y. Q. (2007). Estimating basal area and stem volume for individual trees from LiDAR data. *Photogrammetric Engineering and Remote Sensing, 73*(12), 1355–1365.

Cook, B.D., Corp, L. A., Nelson, R. F., Middleton, E. M., Morton, D. C., McCorkel, J. T., et al. (2013). NASA Goddard's LiDAR, Hyperspectral and Thermal (G-LiHT) Airborne Imager. *Remote Sensing, 5*(8), 4045–4066.

Enquist, B. J. (2002). Universal scaling in tree and vascular plant allometry: Toward a general quantitative theory linking plant form and function from cells to ecosystems. *Tree Physiology, 22*, 1045–1064.

Ferraz, A., Bretar, F., Jacquemoud, S., Gonçalves, G., Pereira, L., Tomé, M., et al. (2012). 3-D mapping of a multi-layered Mediterranean forest using ALS data. *Remote Sensing of Environment, 121*, 210–223.

Hunsaker, C., Boroski, B., & Steger, G. (2002). *Relationships between canopy cover and occurrence and productivity of California spotted owls, predicting species occurrences, issues of accuracy and scale.* Covelo, CA: Island Press.

Kaartinen, H., Hyyppä, J., Yu, X., Vastaranta, M., Hyyppä, H., Kukko, A., et al. (2012). An international comparison of individual tree detection and extraction using airborne laser scanning. *Remote Sensing, 4*(4), 950–974.

Koch, B., Heyder, U., & Weinacker, H. (2003). Detection of individual tree crowns in airborne LiDAR data. *Photogrammetric Engineering & Remote Sensing, 72*(4), 357–363.

Kwak, D., Lee, W., Lee, J., Biging, G., & Gong, P. (2007). Detection of individual trees and estimation of tree height using LiDAR data. *Journal of Forest Research, 12*(6), 425–434.

Leckie, D., Gougeon, F., Hill, D., Quinn, R., Armstrong, L., & Shreenan, R. (2003). Combine high-density LiDAR and multispectral imagery for individual tree crown analysis. *Canadian Journal of Remote Sensing, 29*(5), 633–649.

Lefsky, M.A., Harding, D., Cohen, W. B., Parker, G., & Shugart, H. H. (1999). Surface LiDAR remote sensing of basal area and biomass in deciduous forests of Eastern Maryland, USA. *Remote Sensing of Environment, 67*(1), 83–98.

Maltamo, M., Mustonen, K., Hyyppa, J., Pitkanen, J., & Yu, X. (2004). The accuracy of estimating individual tree variables with airborne laser scanning in a boreal nature reserve. *Canadian Journal of Forest Research, 34*(9), 1791–1801.

Persson, A., Holmgren, J., & Soderman, U. (2002). Detecting and measuring individual trees using an airborne laser scanner. *Photogrammetric Engineering and Remote Sensing, 68*(9), 925–932.

Popescu, S. (2007). Estimating biomass of individual pine trees using airborne LiDAR. *Biomass and Bioenergy, 31*(9), 646–655.

Popescu, S., & Wynne, R. (2004). Seeing the trees in the forest: Using LiDAR and multispectral data fusion with local filtering and variable window size for estimating tree height. *Photogrammetric Engineering and Remote Sensing, 70*(5), 589–604.

Popescu, S., Wynne, R., & Nelson, R. (2003). Measuring individual tree crown diameter with LiDAR and assessing its influence on estimating forest volume and biomass. *Canadian Journal of Remote Sensing, 29*(5), 564–577.

Rahman, M., & Gorte, B. (2009). *Tree crown delineation from high resolution airborne LiDAR based on densities of high points.* Laserscanning09, XXXVIII, Paris, France, 123–128.

Swatantran, A., Dubayah, R., Roberts, D., Hofton, M., & Blair, J. B. (2011). Mapping biomass and stress in the Sierra Nevada using LiDAR and hyperspectral data fusion. *Remote Sensing of Environment, 115*(11), 2917–2930.

Vastaranta, M., Holopainen, M., Yu, X., Haapanen, R., Melkas, T., Hyyppa, J., et al. (2011). Individual tree detection and area-based approach in retrieval of forest inventory characteristics from low-pulse airborne laser scanning data. *Photogrammetric Journal of Finland, 22*(2), 1–13.

Wulder, M., Niemann, K. O., & Goodenough, D.G. (2000). Local maximum filtering for the extraction of tree locations and basal area from high spatial resolution imagery. *Remote Sensing of Environment, 73*(1), 103–114.

Wulder, M.A., White, J. C., Nelson, R. F., Naesset, E., Orka, H. O., Coops, N. C., et al. (2012). LiDAR sampling for large-area forest characterization: A review. *Remote Sensing of Environment, 121*(1), 196–209.

Zolkos, S. G., Goetz, S. J., & Dubayah, R. (2013). A meta-analysis of terrestrial aboveground biomass remote sensing. *Remote Sensing of Environment, 128*, 289–298.